Zero-lag synchronization and multiple time delays in two coupled chaotic systems

Meital Zigzag,[1] Maria Butkovski,[1] Anja Englert,[2] Wolfgang Kinzel,[2] and Ido Kanter[1]
[1]*Department of Physics, Bar-Ilan University, Ramat-Gan 52900, Israel*
[2]*Institute for Theoretical Physics, University of Würzburg, Am Hubland, 97074 Würzburg, Germany*
(Received 22 July 2009; revised manuscript received 8 February 2010; published 23 March 2010)

Zero-lag synchronization (ZLS) between two chaotic systems coupled by a portion of their signal is achieved for restricted ratios between the delays of the self-feedback and the mutual coupling. We extend this scenario to the case of a set of multiple self-feedbacks $\{N_{d_i}\}$ and a set of multiple mutual couplings $\{N_{c_j}\}$. We demonstrate both analytically and numerically that ZLS can be achieved when $\Sigma l_i N_{d_i} + \Sigma m_j N_{c_j} = 0$, where $l_i, m_j \in \mathbb{Z}$. Results which were mainly derived for Bernoulli maps and exemplified with simulations of the Lang-Kobayashi differential equations, indicate that ZLS can be achieved for a continuous range of mutual coupling delay. This phenomenon has an important implication in the possible use of ZLS in communication networks.

DOI: 10.1103/PhysRevE.81.036215 PACS number(s): 05.45.−a

I. INTRODUCTION

Two identical chaotic systems starting from almost identical initial states, end up in completely uncorrelated trajectories [1,2]. On the other hand, chaotic systems which are mutually coupled by some of their internal variables can synchronize to a collective dynamical behavior [3–6]. The mechanism of the ZLS phenomenon has been subject of controversial debate, where the main puzzle is how two or more distant dynamical elements can synchronize at zero-lag even in the presence of non-negligible delays in the transfer of information between them.

The phenomenon of ZLS was also experimentally observed in the synchronization of two mutually coupled chaotic semiconductor lasers, where the optical path between the lasers is a few orders of magnitude greater than the coherence length of the lasers [7–12]. This phenomenon has attracted a lot of attention, mainly because of its potential for secure communication over a public channel [7,13,14]. In [15] it was recently shown that it is possible to use the ZLS phenomenon of two mutually coupled symmetric chaotic systems for a novel key-exchange protocol generated over a public channel. Note that in contrary to a public scheme which is based on mutual coupling, private-key secure communication is based on a unidirectional coupling [16,17] and it is susceptible to an attacker which has identical parameters and is coupled to the transmitted signal. The generation of secure communication over a public channel requires mutual coupling and was only proven to be secure based on the ZLS phenomenon [15].

Recently, it has been shown both numerically and analytically that various architectures of coupled chaotic systems can exhibit ZLS [18–27]. The main disadvantage of this phenomenon is that ZLS even between two mutually coupled chaotic systems can be achieved only for very restricted architectures and it is highly sensitive for mismatch between the delays of the mutual coupling and the self-feedback [28]. These delays have to be identical or have to fulfill special ratios. Such a realization might exist in a time-independent point-to-point communication, but it is far from the realm of communication networks.

In this paper we first demonstrate the constraint that ZLS is achieved only for very restricted ratio between the self-feedback and the mutual delays, $lN_d = mN_c$, where l and m are (small) integers. We next show that one can overcome this constraint when multiple self-feedbacks are used. The extension of the setup with multiple self-feedbacks to include multiple mutual couplings is also discussed and reveals a general condition for the emergence of zero-lag synchronization in mutually coupled delayed chaotic systems, even when the systems have different self-feedback delays. For the simplicity of the presentation we mainly concentrate on the Bernoulli map, where results of simulations can be compared to an analytical solution [21,29]. However we observed the reported phenomena for other chaotic maps and systems as well, and this is exemplified by the ZLS of mutually coupled chaotic semiconductor lasers, depicted by the Lang-Kobayashi differential equations [7,30].

The paper is an extension of [31]. It contains a full detailed description of the analytical methods and simulations of various architectures, new analytical results and relations and discussions that were not included in [31]. The paper is organized as follows: in Sec. II Bernoulli maps with single self-feedback and single mutual coupling are introduced and analyzed. The extension to multiple self-feedbacks is examined in Sec. III, where setups with multiple mutual couplings are examined in Sec. IV. The general scenario of multiple self-feedbacks and multiple mutual couplings is investigated in Sec. V. The extension of the results to mutually coupled chaotic diode lasers depicted by the Lang-Kobayashi differential equations is presented in Sec. VI. The Bernoulli maps in the limit $\varepsilon \to 1$ is examined in Sec. VII and in the Appendix. A short discussion about two Bernoulli maps with different slope is shown in Sec. VIII. A general discussion and a summary of the results is presented in Sec. IX.

II. SINGLE SELF-FEEDBACK AND SINGLE MUTUAL COUPLING

The cornerstone of our system is the simplest chaotic map, the Bernoulli map, $f(x)=(ax) \bmod 1$, which is chaotic for $a>1$. The dynamical equations of two mutually coupled chaotic units, X and Y, with one self-feedback (see Fig. 1) are given by

$$x_n = (1-\varepsilon)f(x_{n-1}) + \varepsilon\kappa f(x_{n-N_d}) + \varepsilon(1-\kappa)f(y_{n-N_c}),$$

$$y_n = (1-\varepsilon)f(y_{n-1}) + \varepsilon\kappa f(y_{n-N_d}) + \varepsilon(1-\kappa)f(x_{n-Nc}), \quad (1)$$

where N_d and N_c are the delays of the self-feedback and the mutual coupling, respectively [21]. The quantities $(1-\varepsilon)$, $\varepsilon\kappa$ and $\varepsilon(1-\kappa)$ stand for the strength of the internal dynamics, self-feedback and the mutual coupling, respectively. $(1-\varepsilon),\varepsilon\kappa,\varepsilon(1-\kappa)\in[0,1]$ and their summation is equal to 1. Note that when there is no coupling between the two units, the entire signal is the internal dynamics, $f(x_{n-1}),f(y_{n-1})$, and the self-feedback, $f(x_{n-Nd}),f(y_{n-Nd})$, i.e., the whole signal goes through the unit and the strength of the mutual coupling is zero, $\kappa=1$. In this case the unit is chaotic.

The solution of the relative distance between the trajectories of the two mutually coupled chaotic Bernoulli maps can be analytically examined [21,29]. Let us denote by δx_n and δy_n small perturbations from the trajectories x_n and y_n, respectively. For a small perturbation we can linearize the equations into

$$\delta x_n = (1-\varepsilon)a\,\delta x_{n-1} + \varepsilon\kappa a\,\delta x_{n-N_d} + \varepsilon(1-\kappa)a\,\delta y_{n-N_c},$$

$$\delta y_n = (1-\varepsilon)a\,\delta y_{n-1} + \varepsilon\kappa a\,\delta y_{n-N_d} + \varepsilon(1-\kappa)a\,\delta x_{n-N_c}. \quad (2)$$

Using the ansatz $\delta x_n = c^n \delta x_0$ and $\delta y_n = c^n \delta y_0$ we can get

$$\begin{pmatrix} 0 & 1 \\ 1 & 0 \end{pmatrix}\begin{pmatrix} \delta x_0 \\ \delta y_0 \end{pmatrix} = \frac{c-(1-\varepsilon)a-\varepsilon\kappa a c^{1-N_d}}{a\varepsilon(1-\kappa)c^{1-N_c}}\begin{pmatrix} \delta x_0 \\ \delta y_0 \end{pmatrix}. \quad (3)$$

This matrix has two eigenvalues $\gamma_1=1$, which describes relaxation perturbations parallel to the synchronization manifold, and $\gamma_2=-1$ which describes relaxation perturbations perpendicular to the synchronization manifold. After substituting γ_2, in order to find the stable solution, one finds that the characteristic polynomial is given by

$$c-(1-\varepsilon)a-\varepsilon\kappa a c^{1-N_d}+\varepsilon(1-\kappa)a c^{1-N_c}=0, \quad (4)$$

where $c=e^{\lambda+i\phi}$ and $\lambda=\ln|c|$ is the Lyapunov exponent. Equation (4) determines the entire spectrum of the Lyapunov exponents of the coupled systems. However, only the exponents transversal to the synchronization manifold are important for the stability of the synchronization. Equation (4) is a polynomial of order $\tau=\max(N_c,N_d)$, therefore it has τ solutions, Lyapunov exponents. The synchronization is stable only when $\lambda_i<0\,\forall\, i$ except the one parallel to the synchronization manifold, hence checking only the maximal one is sufficient.

For small values of $a(1-\varepsilon)$, i.e., $\varepsilon\to 1$, the second term in the LHS of the characteristic polynomial (4) is negligible and the equation is reduced to

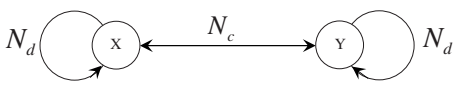

FIG. 1. A schematic of two mutually coupled units at a distance N_c with one self-feedback with a delay equals to N_d.

$$c = a\varepsilon\kappa c^{1-N_d} - a\varepsilon(1-\kappa)c^{1-N_c}. \quad (5)$$

which means that the problem decomposes to a time lattice. Analytical results have been found in [32] with the following ansatz. Using $c=|c|e^{i\phi}$ on the unit circle $|c|=1$, the border to synchronization, this equation is reduced to

$$1 = a\varepsilon\kappa e^{-i\phi N_d} - a\varepsilon(1-\kappa)e^{-i\phi N_c}. \quad (6)$$

This equation describes the border of synchronization (for $\varepsilon\to 1$), since for $|c|<1(|c|>1)$ the maximal Lyapunov exponent is negative (positive) and synchronization is achieved (not achieved). In order to find the solutions for the coefficients $a\varepsilon\kappa$ and $a\varepsilon(1-\kappa)$ beyond which no synchronization is possible we separate Eq. (6) into a real and an imaginary parts,

$$1 = a\varepsilon\kappa\cos(\phi N_d) - a\varepsilon(1-\kappa)\cos(\phi N_c),$$

$$0 = a\varepsilon\kappa\sin(\phi N_d) - a\varepsilon(1-\kappa)\sin(\phi N_c). \quad (7)$$

By taking $|\cos(\phi N_d)|,|\cos(\phi N_c)|=1$ and $\sin(\phi N_d),\sin(\phi N_c)=0$, one can find the upper and lower bounds of κ for which ZLS is achieved in the limit of $\varepsilon\to 1$,

$$\kappa_{\pm} = \frac{a\pm 1}{2a}. \quad (8)$$

On the ZLS borders the two Eqs. (7) have two variables $(\phi N_d,\phi N_c)$, and therefore solvable. These equations have a variety of solutions due to the periodicity of the trigonometric functions, sin and cos, and their solutions have the following form

$$lN_d = mN_c, l,m\in\mathbb{Z}. \quad (9)$$

Obviously this equation is valid for any two integer numbers, N_d and N_c, and does not limit the ratio between them. Observation on the Lyapunov exponents reveals that our condition for ZLS is not sufficient. To be on the ZLS border it is needed that $|c_{max}|=1$ (and not only $|c|=1$). In order to verify whether $|c_{max}|=1$, we solved numerically the characteristic polynomial (4). Results indicate that independent of $10\le N_d\le 40$, $|c_{max}|=1$ is valid in the upper bound only when

$$lN_d = N_c, \quad (10)$$

where l is a bounded integer, and in the lower bound only when

$$N_d = mN_c, \quad (11)$$

where m is a bounded integer. This is consistent with our result in [32]. For instance, for $a=1.1$ and $\varepsilon=1$, $|c_{max}|=1$ is fulfilled only for $m,l<21$. Note that Eqs. (10) and (11) are necessary but not sufficient. However far from the boarder of synchronization, for intermediate values of κ, ZLS is achieved when Eq. (9) is fulfilled, where both m and l are bounded and greater or equal to 1. Results for $a=1.1$ are exemplified in Fig. 2. The left panel is for $\varepsilon=0.98$, $\kappa=0.8$ and the right one for $\varepsilon=0.98$, $\kappa=0.4$. For the left panel, ZLS is achieved for the pairs $(m,l)=(-1,l)$ where $l=1,2,\ldots,10$, $(3,-2)$ and $(3,-1)$. For the right panel ZLS is achieved for the pairs $(-1,l)$ $l=1,\ldots,5$, $(3,-1)$, $(5,-1)$,

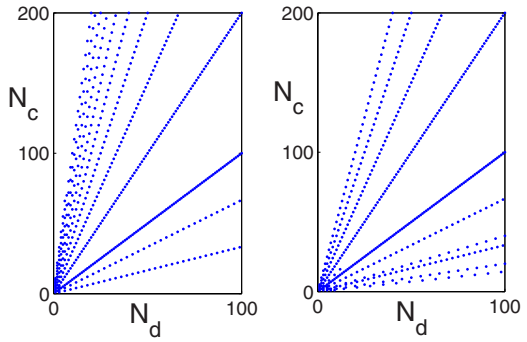

FIG. 2. (Color online) Simulations and semianalytical results for the ZLS points in the parameter space (N_d,N_c) with $a=1.1$, $\varepsilon=0.98$, $\kappa=0.8$ left panel and $a=1.1$, $\varepsilon=0.98$, $\kappa=0.4$ right panel.

$(7,-1)$, $(3,-2)$, and $(5,-2)$. The possible values of l and m depends on the parameters of the model.

In the event that $\varepsilon \nrightarrow 1$, the second term in the LHS of the characteristic polynomial (4) is no longer negligible. This results in width of the straight lines in (N_d,N_c) parameter space, as depicted in Fig. 3 for $a=1.1$, $\varepsilon=0.9$, $\kappa=0.8$ (left panel) and for $a=1.1$, $\varepsilon=0.9$, $\kappa=0.4$ (right panel). For the left panel, ZLS is achieved for the pairs $(m,l)=(-1,l)$ where $l=1,2,\ldots,10$ and $(3,-1)$. For the right panel ZLS is achieved for the pairs $(-1,l)$ $l=1,\ldots,4$, $(3,-1)$, $(5,-1)$, $(7,-1)$, $(3,-2)$, and $(5,-2)$ [33]. Hence the ZLS points are within the enlarged regime $|lN_d-mN_c| \leq \delta(\varepsilon)$, where $\delta(\varepsilon) \approx 2$ for $\varepsilon=0.9$ and is larger for smaller ε.

In order to examine the behavior of the maximal l, l_{max}, for which ZLS is achieved we find l_{max} as a function of $\delta_a=a-1$ by solving semianalytically the characteristic polynomial (4) and simulating the dynamical Eqs. (1) with $\varepsilon=0.999$, so that no extensions and deviations will occur. Results are depicted in Fig. 4 for $\kappa=0.8$ (stars) and $\kappa=0.4$ (dots), with the corresponding linear fits. Results indicate that

$$l_{max} \propto \delta_a^{-\rho} = \frac{1}{(a-1)^{\rho}}, \tag{12}$$

where simulations indicate that

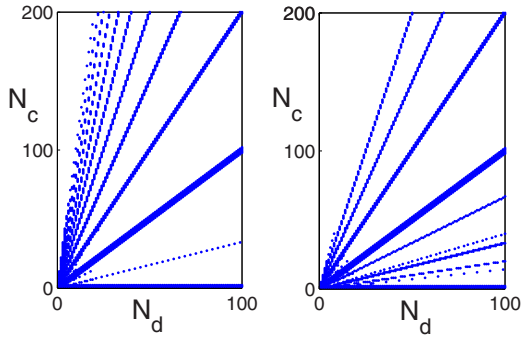

FIG. 3. (Color online) Simulations and semianalytical results for the ZLS points in the parameter space (N_d,N_c) with $a=1.1$, $\varepsilon=0.9$, $\kappa=0.8$ left panel and $a=1.1$, $\varepsilon=0.9$, $\kappa=0.4$ right panel.

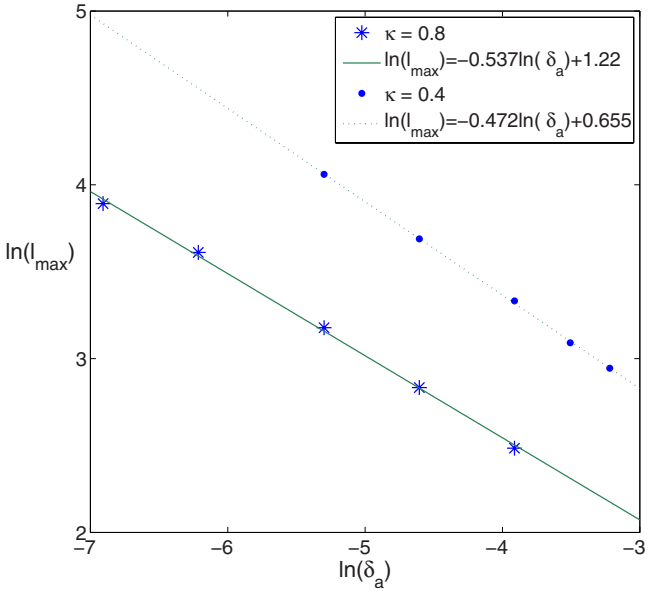

FIG. 4. (Color online) Analytical results of l_{max} as a function of $\delta_a=(a-1)$ with $\varepsilon=0.999$ for $\kappa=0.8$ (stars) and $\kappa=0.4$ (dots). The solid and the dashed lines are the corresponding linear fits.

$$\rho(\kappa) \sim 0.5 \tag{13}$$

and ρ is only weakly dependent on κ. One can also find analytically an upper bound for N_c (see Appendix).

$$N_c < \frac{a(2\varepsilon-1)+1}{a-1}N_d + \frac{2a(\varepsilon-1)}{a-1}, \tag{14}$$

indicating an upper bound for $l_{max} \propto \frac{1}{a-1}$. In the weak chaos limit, $a \to 1^+$, and $\varepsilon \to 1$ we can see that $l_{max} \to \infty$.

More detailed investigations of the case of small ε will be discussed in Sec. VII.

III. MULTIPLE SELF-FEEDBACKS

A. Double self-feedbacks

The constraint (9) indicates that ZLS can be achieved only when N_c is accurately known, which is far from the realm of communication networks. In order to increase the possible ZLS range of N_c for a fixed N_d, we add more self-feedbacks, as depicted in Fig. 5. The generalized dynamical equations for the case of multiple self-feedbacks are given by

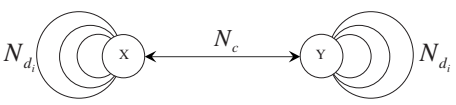

FIG. 5. A schematic of two mutually coupled units at a distance N_c with multiple self-feedbacks.

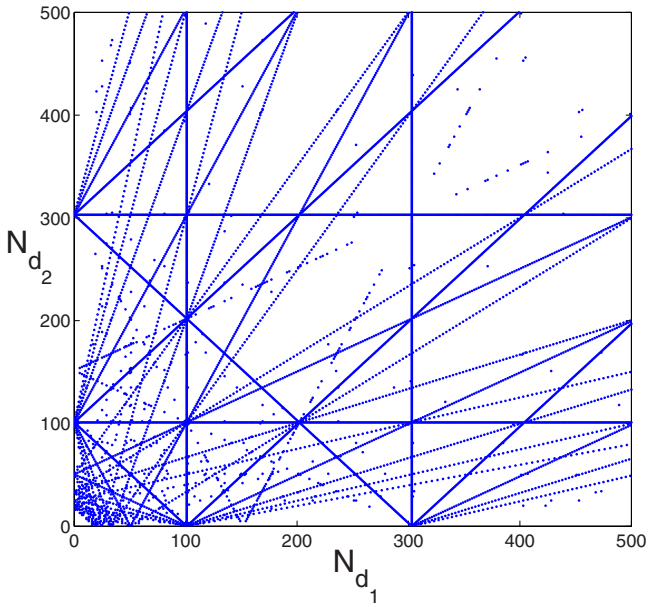

FIG. 6. (Color online) Simulations and semianalytical results for the ZLS points in the parameter space (N_{d_1},N_{d_2}) for $N_c=101$, $a=1.1$, $\varepsilon=0.98$, $\kappa=0.8$, and $\alpha_i=1/2$.

$$x_n=(1-\varepsilon)f(x_{n-1})+\varepsilon\kappa\sum_{i=1}^{M}\alpha_i f(x_{n-N_{d_i}})+\varepsilon(1-\kappa)f(y_{n-N_c}),$$

$$y_n=(1-\varepsilon)f(y_{n-1})+\varepsilon\kappa\sum_{i=1}^{M}\alpha_i f(y_{n-N_{d_i}})+\varepsilon(1-\kappa)f(x_{n-N_c}), \tag{15}$$

where M stands for the number of self-feedbacks and the parameter α_i indicates the weight of the ith self-feedback fulfilling the constraint $\Sigma_{i=1}^{M}\alpha_i=1$. In order to reveal the interplay between possible N_c and a given set of $\{N_{d_i}\}$ which lead to ZLS we first examine in detail the case of $M=2$. In this scenario the characteristic polynomial is

$$c-a(1-\varepsilon)-a\varepsilon\kappa\alpha_1 c^{1-N_{d_1}}-a\varepsilon\kappa\alpha_2 c^{1-N_{d_2}}+a\varepsilon(1-\kappa)c^{1-N_c}=0. \tag{16}$$

Similarly to the simple case, with single self-feedback and single mutual coupling, when $a\varepsilon\to 1$ one can show that far from the border of synchronization ZLS is achieved when

$$l_1N_{d_1}+l_2N_{d_2}=mN_c, \tag{17}$$

where l_1, l_2 and m are bounded integers. Calculation of the largest Lyapunov exponent obtained from the solution of the characteristic polynomial, Eq. (16) which was confirmed by the results of simulations for $\varepsilon=0.98$, is depicted in Fig. 6. It confirms that for $\varepsilon\to 1$ ZLS can be achieved only when Eq. (17) is fulfilled. Numerical solution of the maximal Lyapunov exponent of the characteristic polynomial (16) as well as simulations of the dynamical Eqs. (15) indicate that the same type of solution, Eq. (17), holds also for the entire regime where $|c|<1$.

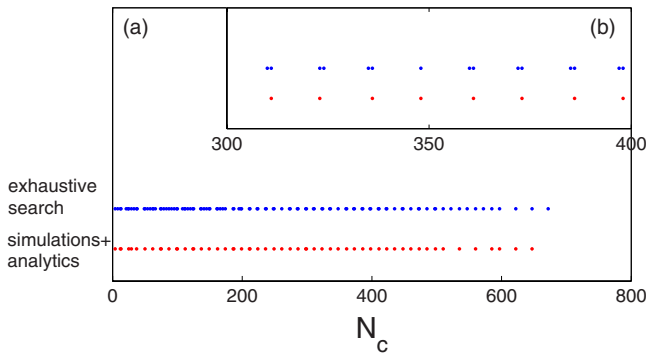

FIG. 7. (Color online) ZLS for two mutually coupled Bernoulli maps with $a=1.1$, $\varepsilon=0.999$ and $\kappa=0.8$ and with two self-feedbacks, $N_{d_1}=25$, $N_{d_2}=87$. ZLS points obtained from the exhaustive search of Eq. (17) with $m=\pm 1,\pm 3$ and l_i in the range $[-6,6]$ (blue points, upper line). The ZLS points obtained from simulation and semianalytical results (red points, lower line). The inset is a blow up of a section of possible N_c with ZLS.

Similarly to the previous section, when $\varepsilon\nrightarrow 1$ the second term in the LHS of the characteristic polynomial (16) is no longer negligible. Simulations and semianalytical calculations results depict that this result in a small width, and the ZLS points are in an enlarged regime $|l_1N_{d_1}+l_2N_{d_2}+mN_c|\le\delta(\varepsilon)$, where $\delta\approx 2$ for $\varepsilon=0.9$ and is larger for smaller ε, see Sec. VII.

Figure 6 indicates that for $\varepsilon=0.98$, $\kappa=0.8$ [34] for instance, m can take the integers ± 1 and ± 3 only. In order to examine the possible range of the integers $\{l_i\}$ we ran an exhaustive search simulation, $-6\le l_i\le 6$ and $m=\pm 1,\pm 3$, and obtained integer N_c from Eq. (17). Figure 7 depicts results of such an exhaustive search and the analytical solution of appropriate characteristic polynomial, for $\varepsilon=0.999$ so that no extensions and deviations will occur. The comparison between the results indicates the following main conclusions: all the ZLS points obtained from the semianalytical calculation (red points, lower line) are achieved also from the exhaustive search (blue points, upper line), i.e., all the semianalytical points are described by Eq. (17), when $-6\le l_i\le 6$ and $m=\pm 1,\pm 3$ and a similar range of N_c was obtained.

We also analyze in detail the case of triple self-feedbacks, Eq. (15) with $M=3$, and find that for $\varepsilon\to 1$ ZLS points follow the equation $l_1N_{d_1}+l_2N_{d_2}+l_3N_{d_3}+mN_c=0$, and in this case the ZLS points form planes. However, when $\varepsilon\nrightarrow 1$ $|l_1N_{d_1}+l_2N_{d_2}+l_3N_{d_3}+mN_c|\le\delta(\varepsilon)$, where $\delta(1)=0$ and increases as ε decreases.

B. Multiple self-feedbacks

The generalization of the characteristic polynomial to the case of multiple self-feedbacks is

$$c-a(1-\varepsilon)-a\varepsilon\kappa\sum_{i=1}^{M}\alpha_i c^{1-N_{d_i}}+a\varepsilon(1-\kappa)c^{1-N_c}=0. \tag{18}$$

Similarly to the previous subsections, when $a\varepsilon\to 1$ one can show that far from the border of synchronization ZLS is achieved when

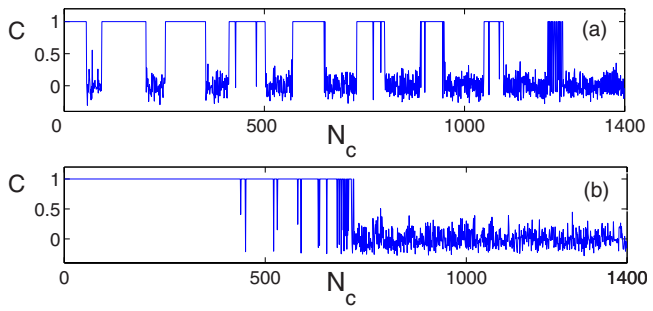

FIG. 8. (Color online) Simulations results of the correlation, C, as a function of N_c for $a=1.1$, $\varepsilon=0.9$ and $\kappa=0.8$ and four $N_{d_i}=11,15,18,150$. The weight of the self-feedbacks, α_i in Eq. (15), are in (a) $\alpha_1=\alpha_2=\alpha_3=0.25/3$ and $\alpha_4=0.75$ and in (b) $\alpha_1=\alpha_2=\alpha_3=0.65/3$ and $\alpha_4=0.35$

$$\sum_{i=1}^{M} l_i N_{d_i} + mN_c = 0, \tag{19}$$

where l_i and m take bounded integer values. This solution holds also in the entire regime where $|c|<1$.

This generalization was indeed confirmed in simulations and solving the characteristic polynomials with up to $M=7$. Below we exemplify the solution of $M=4$, $N_{d_i}=11,15,18,150$. We select one remarkably large N_d such that we can see its effect on the range of N_c where ZLS is achieved. To measure the quality of the ZLS we used the correlation function, which is defined by

$$C = \frac{\langle x_n y_n\rangle - \langle x_n\rangle\langle y_n\rangle}{\sqrt{\langle x_n^2\rangle - \langle x_n\rangle^2}\sqrt{\langle y_n^2\rangle - \langle y_n\rangle^2}}, \tag{20}$$

where $C=1$ indicates complete ZLS and $\langle\ldots\rangle$ stands for an average over the last 1000 time steps. The correlation function, C, obtained in simulations is depicted in Fig. 8 and indicates the following results. Multiple self-feedbacks result in a continuous range of ZLS for N_c, hence it is not required to know exactly the mutual distance (value), N_c. Panel (a) of Fig. 8 indicates that there are at least seven continuous ZLS regimes, each one of them is centered at $150l_4$, where $l_4=0,1,\ldots,6$ and the plateaus are extended $\sim\pm 60$ around the centers (slightly decreases with increasing l_4). This width, ± 60, is much smaller than the ZLS range of the only three short self-feedbacks 11,15,18 which at $\varepsilon=0.9(\delta(\varepsilon)\approx 2)$ was found to be $\sim[1,150]$, indicating that the effective l_1, l_2 and l_3 in Eq. (19) are less than 6. This discrepancy is a result of the dominated weight of $N_4=150$, $\alpha_4=0.75$, in Fig. 8(a). For a smaller weight for the largest delay 150, $\alpha_4=0.35$, panel (b) of Fig. 8, a ZLS is continuously achieved up to $N_c\sim 700$. In this case a weak weight for the largest delay results in limited l_4 which takes the values of 0,1,2,3,4 only, and we expect ZLS in four continuous regimes centered around $N_c=0$, 150, 300, 450, and 600. However these four regimes are now merged by the ± 150 width inspired by the strengthened weight for the short self-feedbacks, $\alpha_1=\alpha_2=\alpha_3=0.65/3$ [35].

In the general case there is an interplay between the following three parameters characterizing the set of the delay times: $N_{d_{max}}$ which is comparable to N_c, $\{N_{d_i}\}\ll N_{d_{max}}$ and $\Delta_i=N_{d_{i+1}}-N_{d_i}$ $i=1,\ldots M-2$, where $\{N_{d_i}\}$ are arranged in an increasing rank order. For instance, the following three sets of four self-feedbacks (2,6,9,150), (11,15,18,150), (80,84,87,150) are characterized by the same $N_{d_{max}}$, Δ_1, and Δ_2. What is the main difference between the ZLS profile of these sets and which set maximizes the continuous range of ZLS? The first set opens only a small continuous ZLS regime [~ 20 for parameters of panel (a)] around $150l_4$, since the time delays are very short. The third set almost does not open a continuous regime of ZLS, since $N_{d_1},N_{d_2},N_{d_3}\gg\Delta_1,\Delta_2$. The maximal continuous ZLS range is achieved when short delays N_{d_1},N_{d_2},N_{d_3} are comparable with $\sim 6\Delta_1,6\Delta_2$ [see Eq. (19)] which is a case of the second set.

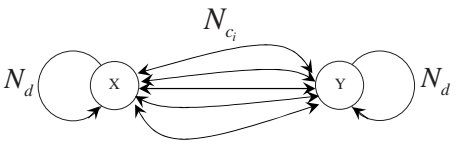

FIG. 9. A schematic of two mutually coupled units with multiple mutual couplings with one self-feedback with a delay equals to N_d.

In the event l_{max} in Eq. (19) is independent of N_{d_i}, one can easily prove that the set

$$N_{d_i} = (2l_{max}+1)^i, \tag{21}$$

where $i=0,1,\ldots,M$ maximizes the continuous range of zero-lag synchronization, $[1,l_{max}\Sigma_{i=1}^{M}(2l_{max}+1)^i]$, however, practically l_{max} is found to be anisotropic, especially in the case of a variety of delays.

Most of the reported simulations were carried out from close initial conditions $(x_n-y_n\approx 10^{-5})$, however, one can find (ε,κ) such that ZLS is achieved from random initial conditions at a comparable synchronization time to ZLS with only one time delay, $N_c=N_d$.

IV. MULTIPLE MUTUAL COUPLINGS

A. Double mutual couplings

In a similar manner to the case of multiple self-feedbacks, one can extend the scenario of multiple self-feedbacks to the case of multiple mutual couplings (see Fig. 9), where the dynamical equations are given by

$$x_n = (1-\varepsilon)f(x_{n-1}) + \varepsilon\kappa f(x_{n-N_d}) + \varepsilon(1-\kappa)\sum_{i=1}^{M}\beta_i f(y_{n-N_{c_i}}),$$

$$y_n = (1-\varepsilon)f(y_{n-1}) + \varepsilon\kappa f(y_{n-N_d}) + \varepsilon(1-\kappa)\sum_{i=1}^{M}\beta_i f(x_{n-N_{c_i}}), \tag{22}$$

where M stands for the number of mutual couplings and the parameter β_i indicates the weight of the ith mutual coupling fulfilling the constraint $\Sigma_{i=1}^{M}\beta_i=1$. In order to reveal the interplay between possible N_d and a given set of $\{N_{c_i}\}$ which lead to ZLS we first examine in detail the case of $M=2$. In this scenario the characteristic polynomial is

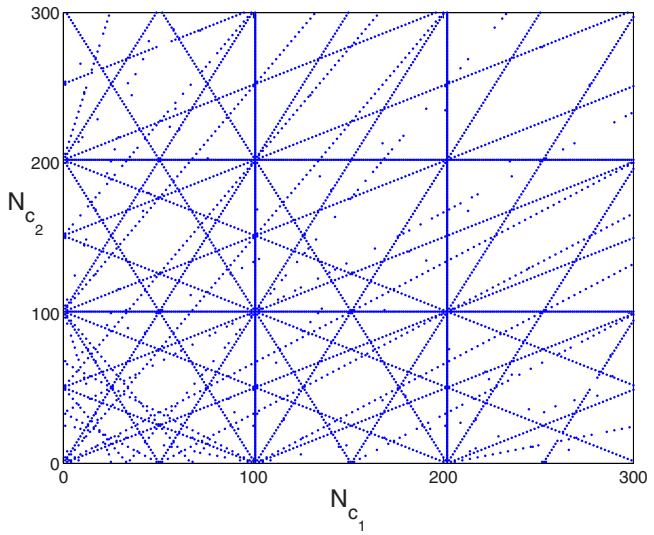

FIG. 10. (Color online) Simulations and semianalytical results for the ZLS points in the parameter space (N_{c_1},N_{c_2}) for $N_d=101$, $a=1.1$, $\varepsilon=0.99$, $\kappa=0.5$ and $\beta_i=1/2$.

$$c-(1-\varepsilon)a-a\varepsilon\kappa\alpha c^{1-N_d}+a\varepsilon(1-\kappa)\beta_1 c^{1-N_{c_1}}+a\varepsilon(1-\kappa)\beta_2 c^{1-N_{c_2}}=0. \tag{23}$$

Similarly to the case of single self-feedback and single mutual coupling with $\varepsilon\to 1$, Sec. II Eqs. (4)–(9), one can show that far from the border of synchronization ZLS is achieved when

$$m_1N_{c_1}+m_2N_{c_2}+lN_d=0, \tag{24}$$

where m_1, m_2 and l take bounded integer values. This solution holds also in the entire regime where $|c|<1$. Figure 10 depicts the points of ZLS for two mutual couplings, N_{c_1} and N_{c_2}, for a given $N_d=101$. Results of simulations were confirmed by the calculation of the largest Lyapunov exponent obtained from the solution of the characteristic polynomial, Eq. (23). The ZLS points (N_{c_1},N_{c_2}) form again straight lines, obeying Eq. (24). For $\varepsilon\to 1$ the lines have a small width, hence a more accurate equation for the ZLS points is $|m_1N_{c_1}+m_2N_{c_2}+nN_d|\le\delta(\varepsilon)$.

A careful examination of Fig. 10 indicates that four lines of ZLS emerge from the origin. These four lines are characterized by

$$\begin{aligned} &m_1=2, \quad m_2=-1, \quad l=0,\\ &m_1=-1, \quad m_2=2, \quad l=0,\\ &m_1=2, \quad m_2=-3, \quad l=0,\\ &m_1=-3, \quad m_2=2, \quad l=0, \end{aligned} \tag{25}$$

indicating that ZLS is achievable independent of N_d. In particular, ZLS is achievable in a face-to-face configuration where $N_{c_2}=2N_{c_1}$ or $2N_{c_2}=3N_{c_1}$ with the lack of a self-feedback $(N_d=0)$, Fig. 17(b) below.

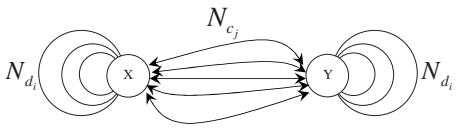

FIG. 11. A schematic of two mutually coupled lasers with multiple self-feedbacks and multiple mutual couplings.

B. Multiple mutual couplings

The generalization of the characteristic polynomial to the case of multiple self-feedbacks is

$$c-a(1-\varepsilon)-a\varepsilon\kappa c^{1-N_{d_i}}+a\varepsilon(1-\kappa)\sum_{i=1}^{M}\beta_i c^{1-N_c}=0. \tag{26}$$

Similarly to the previous section, when $\varepsilon\to 0$ one can show that far from the border of synchronization ZLS is achieved when

$$lN_d+\sum_{i=1}^{M}m_iN_{c_i}=0, \tag{27}$$

where l_i and m take bounded integer values. This solution holds also in the entire regime where $|c|<1$. This generalization was indeed confirmed in simulations and solving the characteristic polynomials with up to $M=7$.

V. MULTIPLE SELF-FEEDBACKS AND MULTIPLE MUTUAL COUPLINGS

A. Identical units

The generalization of the above-mentioned setups to include both multiple self-feedbacks, $\{N_{d_i}\}i=1,\ldots,M_s$ and multiple mutual couplings, $\{N_{c_j}\}j=1,\ldots,M_m$, is straightforward (see Fig. 11). The generalized dynamical equations for this scenario are given by

$$\begin{aligned} x_n&=(1-\varepsilon)f(x_{n-1})+\varepsilon\kappa\sum_{i=1}^{M_s}\alpha_i f(x_{n-N_{d_i}})+\varepsilon(1-\kappa)\sum_{j=1}^{M_m}\beta_j f(y_{n-N_{c_j}}),\\ y_n&=(1-\varepsilon)f(y_{n-1})+\varepsilon\kappa\sum_{i=1}^{M_s}\alpha_i f(y_{n-N_{d_i}})+\varepsilon(1-\kappa)\sum_{j=1}^{M_m}\beta_j f(x_{n-N_{c_j}}), \end{aligned} \tag{28}$$

where M_s and M_m stand for the number of multiple self-feedbacks and multiple mutual couplings, respectively. The parameter α_i indicates the weight of the ith self-feedback and β_j the weight of the jth mutual coupling, fulfilling the constraints $\Sigma_{i=1}^{M_s}\alpha_i=1$ and $\Sigma_{j=1}^{M_m}\beta_j=1$.

Simulation results as well as semianalytical calculation of the (N_{d_1},N_{d_2}) parameter space for double self-feedbacks,

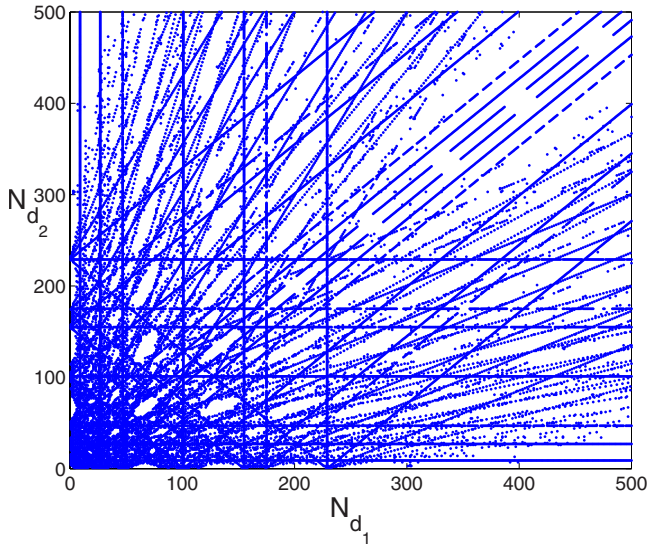

FIG. 12. (Color online) Simulations and semianalytical results for the ZLS points in the parameter space (N_{d_1},N_{d_2}) for double self feedbacks and double mutual couplings with the parameters $N_{c_1}=101$, $N_{c_2}=27$, $a=1.1$, $\varepsilon=0.98$, $\kappa=0.8$, $\alpha_i=1/2$ and $\beta_i=1/2$.

$M_s=2$, and double mutual couplings, $M_m=2$, for fixed N_{c_1}, N_{c_2}, ε, κ, a, α_i and β_i, are depicted in Fig. 12 and indicate that the ZLS lines obey the following generalized equation:

$$\sum_{i=1}^{M_s} l_i N_{d_i} + \sum_{j=1}^{M_m} m_j N_{c_j} = 0, \tag{29}$$

where the lines are characterized by (l_1,l_2,m_1,m_2) and $|l_i| \leq 5$ and $|m_i| \leq 9$.

B. Nonidentical units

The most general setup is where each one of the mutually coupled units has a different set of self-feedback delays. The general dynamical equations are given by

$$x_n = (1-\varepsilon)f(x_{n-1}) + \varepsilon\kappa\sum_{i=1}^{M_s^1} \alpha_i^1 f(x_{n-N_{d_i}^1}) + \varepsilon(1 - \kappa)\sum_{j=1}^{M_m} \beta_j f(y_{n-N_{c_j}}),$$

$$y_n = (1-\varepsilon)f(y_{n-1}) + \varepsilon\kappa\sum_{i=1}^{M_s^2} \alpha_i^2 f(y_{n-N_{d_i}^2}) + \varepsilon(1 - \kappa)\sum_{j=1}^{M_m} \beta_j f(x_{n-N_{c_j}}), \tag{30}$$

where $M_s^1,\{N_{d_i}^1\},\{\alpha_i^1\}$ and $M_s^2,\{N_{d_i}^2\},\{\alpha_i^2\}$ stand for the number of self-couplings, the self-coupling delays and the relative self-coupling weights of the first and the second unit, respectively. Let us first look at the simple scenario of two nonidentical units with single self-feedback, $M_s^1=M_s^2=1$, and single mutual coupling, $M_m=1$, as described in Fig. 13 reveal that only for

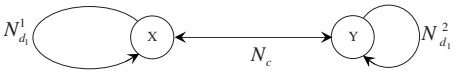

FIG. 13. A schematic of two mutually coupled nonidentical units with single self-feedback and single mutual coupling. N_d^1 and N_d^2 are the self-feedback delays of unit X and Y, respectively. N_c is the mutual delay.

$$N_c = \frac{N_d^1 + N_d^2}{2} \tag{31}$$

and $\kappa=0.5$ the two units are synchronized and with a shift of

$$\Delta = \frac{N_d^1 - N_d^2}{2}, \tag{32}$$

when $x_{n+\Delta}=y_n$, meaning the cross correlation which is defined by

$$C(\Delta) = \frac{\langle x_{n+\Delta}y_n\rangle - \langle x_{n+\Delta}\rangle\langle y_n\rangle}{\sqrt{\langle x_{n+\Delta}^2\rangle - \langle x_{n+\Delta}\rangle^2}\sqrt{\langle y_n^2\rangle - \langle y_n\rangle^2}} \tag{33}$$

is equal to 1 for the aforementioned Δ, see Fig. 14. Semianalytical calculation of the maximal Lyapunov exponent, using the same method as in Eqs. (1)–(4) supports the simulations and indicates that synchronization is achieved with the aforementioned shift. The nonidentical units scenarios are more restricted since for synchronization we demand that the self-feedback and the mutual coupling have the same weight. For instance, here the strength of the self-feedback is $\varepsilon\kappa=0.45$ and the strength of the mutual coupling is $\varepsilon(1-\kappa)=0.45$ as well.

In order to understand the influence of multiple self-feedbacks and multiple mutual couplings on the sets $\{N_{d_i}^1\}$, $\{N_{d_i}^2\}$ and $\{N_c\}$ for which synchronization is achieved, we add another mutual coupling to the previous setup and found the lack of synchronization independent of Δ between the units. However, in the setup of double self-feedbacks, $M_s^1=M_s^2=2$, and double mutual couplings, $M_m=2$, see Fig. 15, synchronization is achieved only when the mutual delays are

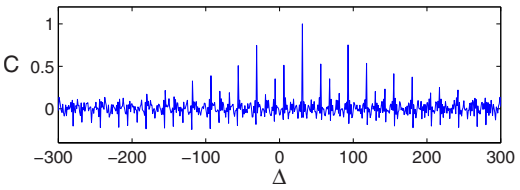

FIG. 14. (Color online) The cross correlation as a function of Δ for two nonidentical units with one self-feedback, $N_d^1=87$, $N_d^2=25$, and one mutual coupling, $N_c=\frac{N_d^1+N_d^2}{2}=56$, with $a=1.1$, $\varepsilon=0.9$ and $\kappa=0.5$. $C(\Delta)=1$ for $\Delta=\frac{N_d^1-N_d^2}{2}=31$.

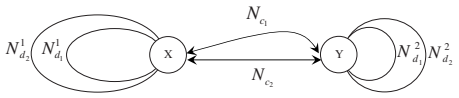

FIG. 15. A schematic of two mutually coupled nonidentical units with double self-feedback and double mutual coupling. $N^1_{d_i}$ are the self-feedback delays of unit X, $N^2_{d_i}$ are the self-feedback delays of unit Y and N_c is the mutual delay.

$$N^1_c = \frac{N^2_{d_1} + N^2_{d_1}}{2},$$

$$N^2_c = \frac{N^2_{d_2} + N^2_{d_2}}{2}, \tag{34}$$

and the self-feedback delays fulfill the equation

$$N^1_{d_1} - N^2_{d_1} = N^1_{d_2} - N^2_{d_2}. \tag{35}$$

In this setup the two units are synchronized with a shift of

$$\Delta = \frac{N^1_{d_1} - N^2_{d_1}}{2} = \frac{N^1_{d_2} - N^2_{d_2}}{2}, \tag{36}$$

when $x_{n+\Delta} = y_n$. An example of such a scenario is depicted in Fig. 16 for the parameters $\varepsilon = 0.9$, $\kappa = 0.5, \alpha^1_i = \alpha^2_i = 0.5$, $\beta_j = 0.5$, $N^1_{d_1} = 87$, $N^1_{d_2} = 131$, $N^2_{d_1} = 25$, $N^2_{d_2} = 69$, $N^1_c = 56$ and $N^2_c = 100$.

Our results indicate that the most general scenario for the emergence of synchronization of two mutually coupled units with time delay couplings is given by

$$\sum_{i=1}^{M^1_s} l^1_i N_{d^1_i} + \sum_{i=1}^{M^2_s} l^2_i N_{d^2_i} + \sum_{j=1}^{M_m} m_j N_{c_j} = 0. \tag{37}$$

Since the synchronization achieved in nonidentical units scenarios is shifted synchronization (and not ZLS as in identical units and as the issue of this paper) we do not explore deeply the scenarios of multiple self-feedbacks and multiple mutual couplings as we do for identical units.

VI. ZLS OF MUTUALLY COUPLED CHAOTIC LASERS

Similar phenomena of ZLS occur in simulations of two mutually coupled semiconductor lasers depicted by the

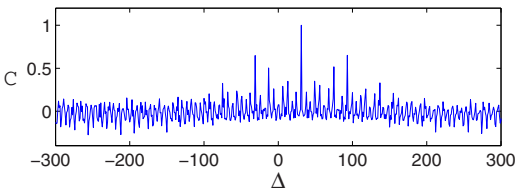

FIG. 16. (Color online) The cross correlation as a function of Δ for two nonidentical units with double self-feedbacks, $N^1_{d_1} = 87$, $N^1_{d_2} = 131$, $N^2_{d_1} = 25$, $N^2_{d_2} = 69$, and double mutual couplings, $N^1_c = (N^2_{d_1} + N^2_{d_1})/2 = 56$, $N^2_c = (N^2_{d_2} + N^2_{d_2})/2 = 100$, with $a = 1.1$, $\varepsilon = 0.9$, $\kappa = 0.5$. $C(\Delta) = 1$ for $\Delta = \frac{N^1_{d_1} - N^2_{d_1}}{2} = \frac{N^1_{d_2} - N^2_{d_2}}{2} = 31$.

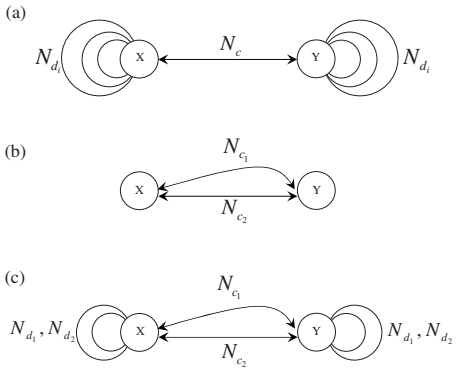

FIG. 17. Schematics of examined setups two mutually coupled chaotic lasers with additional delays: (a) multiple self-feedbacks, (b) double mutual couplings with the lack of self-feedback, (c) double mutual couplings, and double self-feedbacks.

Lang-Kobayashi equations [30]. Our simulations are based on the version and the parameters of these equations as in [7], with additional time delays, Fig. 17.

Figure 18 depicts the ZLS points, correlation > 0.9, in the (N_{d_1}, N_{d_2}) parameter space for double self-feedbacks [Fig. 17(a) with only two self-feedbacks] with the parameters: $N_c = 32$ ns and $\kappa_1 = \kappa_2 = \sigma = 50$ ns^{-1}, where κ_i and σ stand for the intensity of the self-feedbacks and the mutual coupling, respectively. For each (N_{d_1}, N_{d_2}) point the duration of the simulation was 3000 ns and the emergence of ZLS was estimated from the measured cross correlation of the last 20 windows of 100 ns [36]. This figure demonstrates that the ZLS points form straight lines following Eq. (17), similarly to the corresponding maps scenario. The main lines appearing correspond the triplets $(l_1, l_2, m) = (2, -2, 1), (2, -1, -1), (-3, 1, 1), (1, 1, -m)$, where $m = 1, 3$ and $(l_1, 0, -1), (l_1, -1, 1)$, where $l_1 = 1, 2$, and the corresponding triplets with l_2, due to the symmetry. Figure 19 depicts the ZLS as a function of N_c for multiple self-feedbacks, as described in Fig. 17(a). Figure 19(a) examined the case of four time delays $N_{d_i} = 3, 4, 5, 20$ ns and $\kappa_i = \sigma = 30$ ns^{-1} and Fig. 19(b) the case of 6 time delays $N_{d_i} = 11, 12, 13, 14, 15, 16$ ns with $\kappa_i = \sigma$

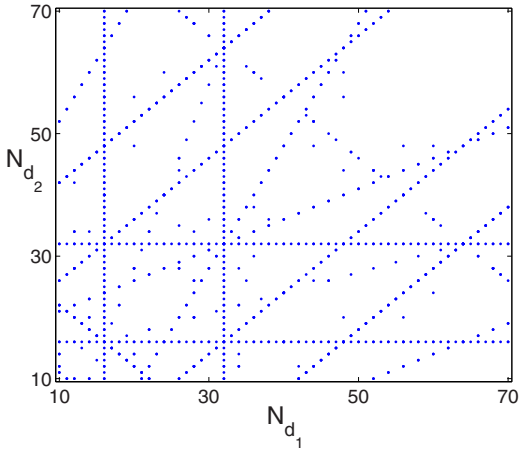

FIG. 18. (Color online) Simulations results for the ZLS points, correlation > 0.9, in the parameter space (N_{d_1}, N_{d_2}) for $N_c = 32$ ns, $\kappa_1 = \kappa_2 = \sigma = 50$ ns^{-1} and $p = 1.02$.

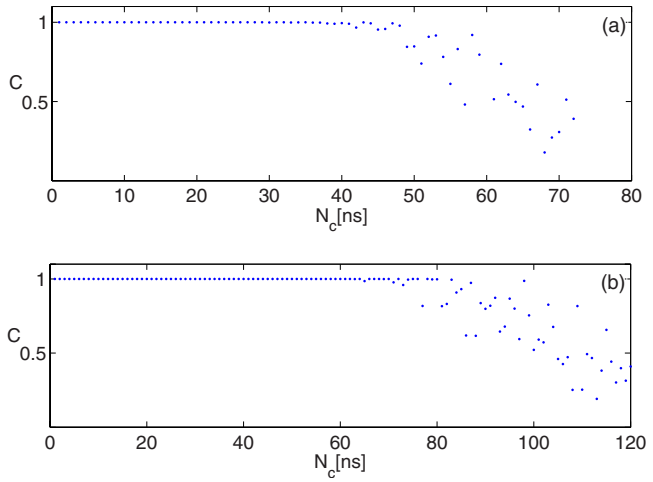

FIG. 19. (Color online) Simulation results of the correlation, Eq. (20), for two mutually coupled semiconductor lasers (details in the text). Panel (a) for four delays $N_d=3,4,5,20$ ns and panel (b) for six time delays $N_d=11,12,13,14,15,16$ ns.

$=25$ ns^{-1}, where for all cases the relative operation pump current with respect to the laser threshold is $p=1.02$. For each N_c the duration of the simulation was 7000 ns and the emergence of ZLS was estimated from the measured cross correlation of the last 20 windows of 100 ns [36]. Results indicate that for the case of six delays ZLS is achieved in the range $\sim[1,80]$ ns where for the case of 4 time delays for $\sim[1,45]$ ns [37]. These synchronization regimes can be explained by Eq. (19) with $l_i=0,\pm 1,\pm 2$ only. It is consistent with our simulations of only one time delay where ZLS is achieved for $N_c=lN_d$ with $l=1,2,3$ only (in contrast to maps where l_i can be much larger, see Figs. 2–8).

The ZLS presented in Figs. 19(a) and 19(b), forms a one-dimensional grid, and no extension and broadening on a time scale of ns is expected, as for discrete-time maps, $\delta\sim 2$. Preliminary results of our simulations indicate that a similar phenomenon occur for a setup consisting of one large self-feedback, $N_{d_{max}}$, and a few short self-feedbacks fulfilling the constraint $\Delta_i=N_{d_{i+1}}-N_{d_i}\sim 0.01$ ns, which is comparable with the coherence time of the semiconductor lasers [9]. In such an event, ZLS is achievable in a continuous range of $N_c\sim N_{d_{max}}\pm O(1$ ns), since the space of the grid is within the coherence time. Hence, the presented mechanism of multiple short-delay self-feedbacks might be implemented in an experiment of mutually coupled chaotic semiconductor lasers using distributed self-feedbacks, and presents the robustness of ZLS under an inaccurate measure of the distance between the mutually coupled lasers [28].

As have been shown, two maps with double mutual couplings such that $N_{c_2}=2N_{c_1}$ are synchronized for every N_d and also stabilize the face-to-face configuration, Fig. 17(b). We observed this phenomenon also in simulations of mutually coupled chaotic semiconductor lasers. For instance, simulations of two chaotic lasers in face-to-face with double mutual couplings with the lack of self-feedbacks, Fig. 17(b), with the parameters $N_{c_1}=13$ ns, $N_{c_2}=26$ ns and also for $N_{c_1}=100$ ns, $N_{c_2}=200$ ns, when $\sigma_1=50$ ns^{-1} and σ_2 was checked for different values: $20,30,\ldots,80$ ns^{-1}. In all cases

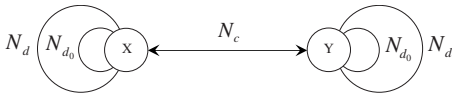

FIG. 20. A schematic of two mutually coupled units at a distance N_c with one self-feedback with a delay equals to N_d, and with additional delay $N_{d_0}=1$ due to the internal dynamics.

ZLS was achieved, $C\approx 1$ [see definition in Eq. (20) for continuous time].

We also obtain ZLS between two mutually coupled semiconductor lasers with double self-feedbacks and double mutual couplings, Fig. 17(c), such that Eq. (29) is fulfilled: $N_{d_1}=7$ ns, $N_{d_2}=9$ ns, $N_{c_1}=11$ ns and $N_{c_2}=27$ ns with $\sigma_i=20$ ns^{-1}, $\kappa_i=40$ ns^{-1} and $p=1.02$.

Synchronization can be achieved also in the general setup, where each one of the semiconductor lasers has a different self-feedback delay, see Fig. 13. Simulation results indicate that similarly to mutually coupled maps, the two semiconductor lasers are synchronized only for $N_c=\frac{N_d^1+N_d^2}{2}$ and with a shift of $\Delta=\frac{N_d^1-N_d^2}{2}$. A similar setup was experimentally and numerically examined with mutually coupled electro-optics oscillators by adding a mirror in the coupling path [38] and was discussed in the concept of simultaneous bidirectional message transmission between two semiconductor lasers [39].

VII. LIMIT $\varepsilon \ll 1$

As shown in the previous sections the accurate straight lines with no width appear only for $\varepsilon\to 1$. Taking ε not close to 1 results in two effects: extension of the ZLS lines ($\delta>1$) and deviations from the integer multiplication between N_{d_i} and N_{c_j} Eq. (29).

The explanation is rooted in understanding that the internal dynamics $(1-\varepsilon)f(x_{n-1})$ and $(1-\varepsilon)f(y_{n-1})$ is in fact another self-feedback equals to 1, $N_{d_0}=1$ (see Fig. 20).

Hence the more accurate equation with a non-negligible strength for the internal dynamics with an additional effective self-feedback, $N_{d_0}=1$, is

$$l_0+\sum_{i=1}^{M_s} l_i N_{d_i}+\sum_{j=1}^{M_m} m_j N_{c_j}=0, \tag{38}$$

where l_0 is a bounded integer. For $\varepsilon\to 1$ the weight of the N_{d_0} is weak, $l_0=0$, and its effect is invisible. However, as depicted in Fig. 8, when one self-feedback, N_{d_i}, has more strength than the others its l_i is larger than the others. Consequently, for $\varepsilon\nrightarrow 1$ $l_0>0$, and deviations from Eq. (29) and $\delta>0$ extension are visible. This can explain the straight horizontal line $N_c=1$ independent of N_d in Fig. 3, which is due to $N_c=N_{d_0}=1$.

Figure 21 demonstrates the changing of the ZLS regimes in the (N_d,N_c) parameter space as ε sails from 1 toward 0. As ε becomes smaller the less lines appear and δ grows, until $\varepsilon=0.1$ where only two wide lines remain $N_c=N_d$ and $N_c=N_{d_0}=1$.

One can also see deviations from Eq. (29) with no extensions for specific sets of ε, κ and a. For the scenario of single

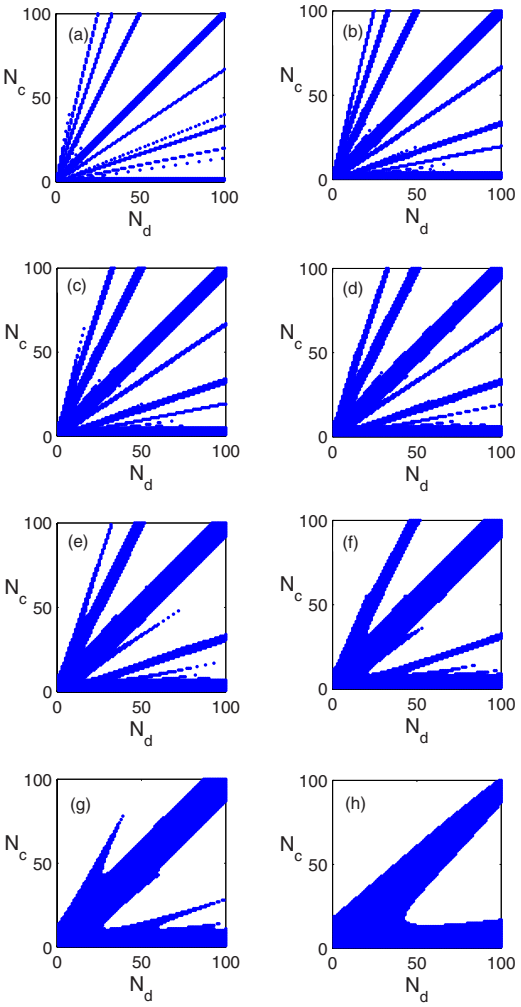

FIG. 21. (Color online) Simulations and semianalytical results for the ZLS points in the parameter space (N_d, N_c) with $a=1.1$, $\kappa=0.4$ (a) $\varepsilon=0.9$, (b) $\varepsilon=0.7$, (c) $\varepsilon=0.6$, (d) $\varepsilon=0.5$, (e) $\varepsilon=0.4$, (f) $\varepsilon=0.3$, (g) $\varepsilon=0.2$, (h) $\varepsilon=0.1$.

self-feedback and single mutual coupling we run on N_c and $-d=-a\varepsilon(1-\kappa)$ for fixed $a(1-\varepsilon)=0.3$, $a\varepsilon\kappa=0.77$ and $N_d=10$, see Fig. 22. We find out that as expected the peaks do not always occur exactly where Eq. (9) is fulfilled. For instance, one peak in Fig. 22 occurs in $N_c=62$ and $-d=-a\varepsilon(1-\kappa)=0.167$. Simulations and semianalytical calculation of the ZLS in the (N_d, N_c) parameter space with those

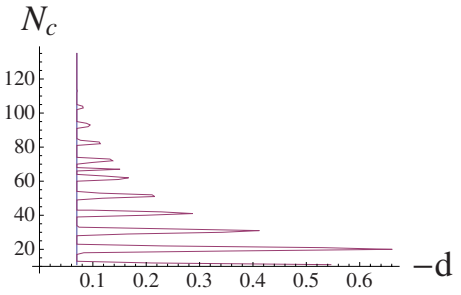

FIG. 22. (Color online) $(N_c, -d)$ parameter space for the parameters $a(1-\varepsilon)=0.3$, $a\varepsilon\kappa=0.77$ and $N_d=10$. The area between the straight line and the curve is where ZLS is achieved.

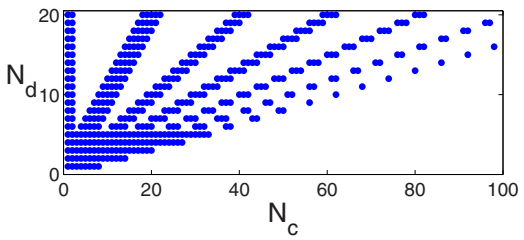

FIG. 23. (Color online) (N_c, N_d) parameter space for the parameters $a(1-\varepsilon)=0.3$, $a\varepsilon\kappa=0.77$ and $-d=-a\varepsilon(1-\kappa)=0.167$.

parameters, are depicted in Fig. 23, indicating that the line described by $N_c=5Nd$ deviates to $N_c=5Nd+1$ and the line $N_c=6Nd$ deviates to $N_c=6Nd+2$. Those deviations are due to the local self-feedback.

The same two effects of deviations and extension are demonstrated in Figs. 24(a) and 24(b) which corresponds to the case of multiple self-feedbacks with the parameters of Figs. 8(a) and 8(b) relatively.

This phenomenon that the internal dynamics can be expressed as $N_{d_0}=1$ is relevant to maps but not to differential equations, such as the Lang-Kobayashi equations. For differential equations the internal dynamics is due to the state of the system at time $t-dt$ where $dt\to 0$. For instance in the examined cases of the mutually coupled chaotic lasers, Sec. VI, $dt \leq 10^{-13}$ s and the delays are of the order of $O(1$ ns).

VIII. DETUNING

The equations of two mutually coupled Bernoulli maps, X and Y, with two different slopes, are given by Eqs. (1) with a_x and a_y, respectively. In this case the analytical solution indicates that ZLS is achieved only for $\varepsilon=1$, $\kappa=0.5$ independent of a_x and a_y. For these parameters there is no internal dynamics, the self-feedback and the mutual coupling have the same strength and therefore X and Y are synchronized. Since for $a_x \neq a_y$ the synchronized state is not a solution of the dynamics, we have numerically examined the difference between the two trajectories for fixed $a_x=1.1$ and three values of $a_y=1.12, 1.2, 1.5$. Figure 25 depicts the region in the parameter space (ε, κ) where the difference between X_n and Y_n averaged over the last 30 000 time steps is less than 0.01, panel (a) and less than 0.001, panel (b). Re-

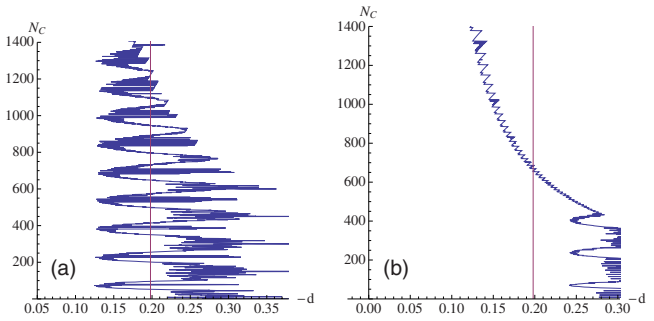

FIG. 24. (Color online) $(N_c, -d)$ parameter space for the same parameters as in Figs. 8(a) and 8(b) relatively. The vertical lines corresponds to the graphs shown in Figs. 8(a) and 8(b).

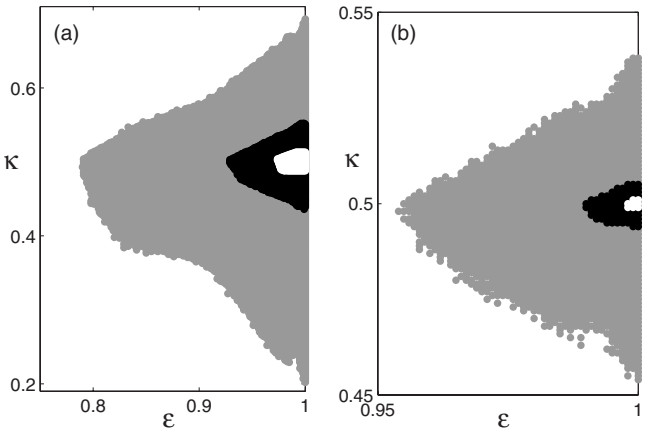

FIG. 25. Simulation results for two mutually coupled Bernoulli maps with different slopes, for $N_c=N_d=80$, $a_x=1.1$ and $a_y=1.12$ (gray), $a_y=1.2$ (black) and $a_y=1.5$ (white). The parameter space (ε,κ) where the difference between X_n and Y_n averaged over the last 30 000 time steps is less than 0.01 is shown in panel (a) and less than 0.001 in panel (b). Notice that the two panels have different scales.

sults indicate that the region in the parameter space increases as a_y-a_x decreases. Similar detuning was experimentally examined on semiconductor lasers in [40].

IX. DISCUSSION

The main conclusion of this paper is that when using additional delays ZLS is achieved when the delays follow Eq. (38). Therefore, additional delays enlarge the range of N_{d_i},N_{c_j} for which ZLS is achieved. We end this paper with a possible physical argument to understand the condition for the emergence of ZLS in the above mutually coupled chaotic units. Each chaotic unit absorbs signals from the history of its own dynamics and from the history of the dynamics of its mutually coupled partner. The output of the chaotic unit blends in a nonlinear fashion the entire input signals together with the current state of the unit itself. For a moment, let us forget the chaotic behavior of the unit and let us assume that the unit acts as a fully transparent unit and/or as a mirror. In such a case, Eq. (5) immediately reveal that the condition $N_c=N_d$ is fulfilled, by passing few times through the units. The fact that the unit is chaotic is expressed in the change of the structure of the chaotic signal, where the shifted correlation function, defined in Eq. (20), reveals some correlations following all periodicity as transparent unit or as a mirror. This is a generic phenomenon which has applications to communication since it is no longer needed to demand $N_c=N_d$ or know precisely the distance between the two systems. As to nonidentical units, which have different sets of $\{N_{d_i}\}$, the delays must follow Eq. (37) and the units are synchronized with a shift. However, extensions to networks consisting of more than two units are still an open question and deserves further research.

ACKNOWLEDGMENT

The research of I.K. is partially supported by the Israel Science Foundation.

APPENDIX

Let us consider the simple system of two mutually coupled units with single self-feedback and single mutual coupling, described by the characteristic polynomial (4). One solution of the system at the edge of synchronization, $|c|=1$, is $\phi=0$, a solution which is always valid and independent of the delay times. However, for $\phi\to 0$ we can calculate an upper bound for l of Eq. (9) and also the corresponding upper bounds for l_i-values for extended systems. Analog to Eq. (7) we split the characteristic polynomial into a real and an imaginary parts and get

$$\cos(\phi N_c) = a(1-\varepsilon)\cos[\phi(N_c-1)] + a\varepsilon\kappa\cos[\phi(N_c-N_d)] - a\varepsilon(1-\kappa),$$

$$\sin(\phi N_c) = a(1-\varepsilon)\sin[\phi(N_c-1)] + a\varepsilon\kappa\sin[\phi(N_c-N_d)]. \tag{A1}$$

By rearranging those equations and using the approximation $\sin(x)\approx x$ for $x\to 0$ one can get an upper bound for N_c,

$$N_c = \frac{a(2\varepsilon-1)+1}{a-1}N_d + \frac{2a(1-\varepsilon)}{a-1}, \tag{A2}$$

By comparing Eqs. (A2) and (9) we can easily see that we also gain an upper bound for l with this formula.

[1] H. G. Schuster and W. Just, *Deterministic Chaos* (Wiley VCH, Weinheim, 2005).
[2] S. Boccaletti, J. Kurths, G. Osipov, D. L. Valladares, and C. S. Zhou, Phys. Rep. **366**, 1 (2002).
[3] A. Pikovsky, M. Rosenblum, and J. Kurths, *Synchronization: A Universal Concept in Nonlinear Sciences* (Cambridge University Press, New York, 2001).
[4] T. L. Carroll and L. M. Pecora, IEEE Trans. Circuits Syst. **38**, 453 (1991).
[5] L. M. Pecora and T. L. Carroll, Phys. Rev. A **44**, 2374 (1991).
[6] L. M. Pecora and T. L. Carroll, Phys. Rev. Lett. **64**, 821 (1990).
[7] E. Klein, N. Gross, E. Kopelowitz, M. Rosenbluh, L. Khaykovich, W. Kinzel, and I. Kanter, Phys. Rev. E **74**, 046201 (2006).
[8] R. Vicente, T. Perez, and C. R. Mirasso, IEEE J. Quantum Electron. **38**, 1197 (2002).
[9] Y. Aviad, I. Reidler, W. Kinzel, I. Kanter, and M. Rosenbluh, Phys. Rev. E **78**, 025204(R) (2008).
[10] I. Fischer, R. Vicente, J. M. Buldu, M. Peil, C. R. Mirasso, M. C. Torrent, and J. Garcia-Ojalvo, Phys. Rev. Lett. **97**, 123902 (2006).
[11] V. Ahlers, U. Parlitz, and W. Lauterborn, Phys. Rev. E **58**, 7208 (1998).

[12] I. Kanter, N. Gross, E. Klein, E. Kopelowitz, P. Yoskovits, L. Khaykovich, W. Kinzel, and M. Rosenbluh, Phys. Rev. Lett. **98**, 154101 (2007).
[13] I. Fischer, Y. Liu, and P. Davis, Phys. Rev. A **62**, 011801(R) (2000).
[14] S. Boccaletti, V. Latora, Y. Moreno, M. Chavez, and D.-U. Hwang, Phys. Rep. **424**, 175 (2006).
[15] I. Kanter, E. Kopelowitz, and W. Kinzel, Phys. Rev. Lett. **101**, 084102 (2008).
[16] G. D. VanWiggeren and R. Roy, Science **279**, 1198 (1998).
[17] A. Argyris *et al.*, Nature (London) **438**, 343 (2005).
[18] F. M. Atay, J. Jost, and A. Wende, Phys. Rev. Lett. **92**, 144101 (2004).
[19] E. Rodriguez, N. George, J. P. Lachaux, J. Martinerie, B. Renault, and F. J. Varela, Nature (London) **397**, 430 (1999).
[20] G. Schneider and D. Nikolic, J. Neurosci. Methods **152**, 97 (2006).
[21] J. Kestler, E. Kopelowitz, I. Kanter, and W. Kinzel, Phys. Rev. E **77**, 046209 (2008).
[22] M. J. Bünner and W. Just, Phys. Rev. E **58**, R4072 (1998).
[23] M. G. Earl and Steven H. Strogatz, Phys. Rev. E **67**, 036204 (2003).
[24] C. Masoller and A. C. Martí, Phys. Rev. Lett. **94**, 134102 (2005).
[25] M. Dhamala, V. K. Jirsa, and M. Ding, Phys. Rev. Lett. **92**, 074104 (2004).
[26] I. B. Schwartz and L. B. Shaw, Phys. Rev. E **75**, 046207 (2007).
[27] M. Chen and J. Kurths, Phys. Rev. E **76**, 036212 (2007).
[28] To achieve ZLS between two semiconductor lasers it was found that the mismatch between N_d and N_c has to be smaller than the coherence time, less than 1 mm [7,9]. Hence, the relative error in the measurement of N_c has to be of the order of 10^{-8} over a distance of 100 km, and might also be sensitive to the time-dependent features of the environment.
[29] S. Lepri, G. Giacomelli, A. Politi, and F. T. Arecchi, Physica D **70**, 235 (1994).
[30] R. Lang and K. Kobayashi, IEEE J. Quantum Electron. **QE-16**, 347 (1980).
[31] M. Zigzag, M. Butkovski, A. Englert, W. Kinzel, and I. Kanter, Euro phys. Lett. **85**, 60005 (2009).
[32] W. Kinzel, A. Englert, G. Reents, M. Zigzag, and I. Kanter, Phys. Rev. E **79**, 056207 (2009).
[33] Even integers m appear, for instance, for $\varepsilon=0.2$, $\kappa=0.6$ where ZLS is achieved for $(2,-3)$ and $(2,-5)$. The range of (m,l) diverges in the limit of weak chaos $a\rightarrow 1^{+}$.
[34] Note that the weight of the mutual coupling is $\varepsilon(1-\kappa)=0.196$ but the effective weight of one self-feedback is $\varepsilon\kappa\alpha_i=0.392$. Hence, the ZLS is not expected to be equal to either panels of figure 3.
[35] The semianalytical solution indicates that plateaus of ZLS are slightly wider and no few sudden drops among the plateaus. These tiny mismatches are due to almost zero maximal Lyapunov exponent close to the plateaus boundaries, and limited number of steps in simulations.
[36] For relative operation pump current with respect to the laser threshold $p=1.02$, chaotic signals consist of low frequency fluctuations (LFFs) where short desynchronizations occur with the used numerical integration 10^{-14}, see also [7]. We avoid this affect by calculating the average cross correlation [Eq. (20)] of the maximal 10 among last 20 windows of size 100 ns each.
[37] Our results are in disagreement with the reported results of E. M. Shahverdiev and K. A. Shore, Phys. Rev. E **77**, 057201 (2008).
[38] M. Peil, L. Larger, and I. Fischer, Phys. Rev. E **76**, 045201(R) (2007).
[39] R. Vicente, C. R. Mirasso, and I. Fischer, Opt. Lett. **32**, 403 (2007).
[40] N. Gross, W. Kinzel, I. Kanter, M. Rosenbluh, and L. Khaykovich, Opt. Commun. **267**, 464 (2006).